Global nuclear reorganization during heterochromatin replication in the giant-genome plant *Nigella damascena* L.

Eugene A. Arifulin[1], Dmitry V. Sorokin[2], Nadezhda A. Anoshina[2], Maria Kuznetsova[3], Anna A. Valyaeva[1,4,5], Anna V. Fedotova[1,8], Veit Schubert[6], Tatyana D. Kolesnikova[7], Eugene V. Sheval[1,5]

[1]*Belozersky Institute of Physico-Chemical Biology, Lomonosov Moscow State University, Moscow, Russia*

[2]*Laboratory of Mathematical Methods of Image Processing, Faculty of Computational Mathematics and Cybernetics, Lomonosov Moscow State University, Moscow, Russia*

[3]*Florey Institute of Neuroscience and Mental Health, Melbourne Brain Centre, University of Melbourne, Parkville, Victoria, Australia*

[4]*School of Bioengineering and Bioinformatics, Lomonosov Moscow State University, Moscow, Russia*

[5]*Department of Cell Biology and Histology, School of Biology, Lomonosov Moscow State University, Moscow, Russia*

[6]*Leibniz Institute of Plant Genetics and Crop Plant Research (IPK) Gatersleben, D-06466 Seeland, Germany*

[7]*Institute of Molecular and Cellular Biology SB RAS, 630090 Novosibirsk, Russia*

[8]*Skolkovo Institute of Science and Technology, Moscow, Russia*

ORCIDs:

Eugene A. Arifulin	0000-0002-3695-4215
Dmitry V. Sorokin	0000-0003-3299-2545
Nadezhda A. Anoshina	0009-0004-7831-6256
Maria Kuznetsova	0000-0001-9646-0121
Anna A. Valyaeva	0000-0003-0304-1206
Veit Schubert	0000-0002-3072-0485
Tatyana D. Kolesnikova	0000-0002-5107-1445
Eugene V. Sheval	0000-0003-1687-1321

Abbreviations

EdU, 5-ethynyl-2′-deoxyuridine
3D-SIM, Three-dimensional structured illumination microscopy
CLEM, Correlative light and electron microscopy
TEM, Transmission electron microscopy

Abstract

Among land plants, genome sizes vary remarkably by > 2,200-fold. This variation depends on the loss and gain of non-coding DNA sequences, forming different heterochromatin complexes during interphase. In plants with a giant genome, the major part of chromatin stays condensed in interphase, forming a dense meshwork of heterochromatin threads, called interphase

chromonemata. Using super-resolution light and electron microscopy, we studied the ultrastructure of chromonemata during and after replication in root meristem nuclei of *Nigella damascena* L. During S-phase, heterochromatin undergoes transient decompaction locally at the active sites of DNA synthesis, and due to the heterochromatin abundance, chromonema replication is accompanied by a robust chromonema meshwork disassembly, which led to the general reorganization of the nucleus morphology visible even by conventional light microscopy. After replication, the heterochromatin condenses again, restoring the chromonema structure. Thus, we showed that heterochromatin replication in interphase nuclei of giant-genome plants induces a global chromonema decondensation and reorganization.

Introduction

Genomic DNA in eukaryotes is hierarchically organized and compacted within interphase nuclei via interacting with different cations, proteins, and RNAs, forming diverse morphological complexes generally referred to as chromatin. At the first level of chromatin organization, ~147 bp DNA fragments are wrapped around core histone octamers to form nucleosome fibers, which have a diameter of about ~11 nm (Kornberg, 1974; Olins and Olins, 1974). For a long time, it was thought that the nucleosome fibers compact into 30-nm fibers, but data from cryo-electron microscopy proved they do not exist in living cells (McDowall *et al.*, 1986; Eltsov *et al.*, 2008; Maeshima *et al.*, 2014). Additionally, thicker fibers of 100-130 nm (Sparvoli *et al.*, 1965; Marsden and Laemmli, 1979; Zatsepina *et al.*, 1983; Belmont and Bruce, 1994) and 200-250 nm (Strukov *et al.*, 2003; Kireeva *et al.*, 2004) in diameter were also observed. However, the higher-order chromatin organization is still under debate (Beseda *et al.*, 2020; Câmara et al., in revision).

In interphase nuclei, chromatin can be divided into two major fractions - euchromatin and heterochromatin. Heterochromatin is transcriptionally inactive and includes chromosome regions containing inactive genes and regions enriched with non-coding sequences (including various transposable elements). These findings correlate well with data from chromosome conformation capture sequencing (Hi-C), indicating that interphase chromatin is partitioned in animals into active A- and repressed B-compartments (Lieberman-Aiden *et al.*, 2009). A- and B-compartments were also detected in interphase nuclei of some plants with small genome sizes ranging from 0.4 to 2.4 Gbp/1C.

The distribution and shape of heterochromatin complexes may vary in cells and tissues. In the majority of mammalian species, small blocks of heterochromatin are located preferentially at the nuclear periphery in contact with the nuclear envelope and around nucleoli (perinucleolar chromatin) (Solovei *et al.*, 2016; van Steensel and Belmont, 2017). Also, in plants, e.g., *Arabidopsis* such a distribution is evident (Schubert *et al.*, 2012). However, a unique exception was found in the rod photoreceptors of nocturnal mammals, in which euchromatin and heterochromatin exchanged their positions (Solovei *et al.*, 2009; Falk *et al.*, 2019; Feodorova *et al.*, 2020). The data obtained predominantly from animals, especially mammals may not reflect chromatin organization in plants. It seems that considerably diverse heterochromatin structures occur in plants (Nagl and Bachmann, 1980).

The genome size in mammals varies only slightly (Gregory, 2011; Redi and Capanna, 2012; Kapusta *et al.*, 2017). However, a huge disparity in genome size and complexity occurs across diverse plant species (Michael, 2014; Pellicer and Leitch, 2020). Among land plants, genome sizes vary remarkably by > 2,200-fold, ranging from 67.2 Mbp/1C *Genlisea aurea* (Fleischmann *et al.*, 2014) to 149.185 Gbp/1C in *Paris japonica* (Pellicer *et al.*, 2010). Variation in genome size in green plants depends, at least partially, on whole-genome duplication, which is widespread in plants (Van de Peer *et al.*, 2017; Li *et al.*, 2021). But the majority is caused by the gain and loss of transposable elements. Indeed, there is a linear

relationship between plant genome size and transposable element content at a given ploidy level (Lee and Kim, 2014).

It seems that the genome size increase modifies also the nuclear organization. In interphase nuclei, the amount of condensed chromatin increases with genome size and may influence the general heterochromatin distribution pattern (Nagl and Bachmann, 1980). Three interphase nuclei patterns, differing in quantity, morphology, and localization of heterochromatin, were described in plants via electron microscopy.

Heterochromatin in different species can form (i) chromocenters, or (ii) chromomeres, or (iii) chromonemata (Nagl and Fusenig, 1979; Nagl and Bachmann, 1980; Nagl *et al.*, 1983).

(i) In small-genome plants (<1 Gbp/1C), the heterochromatin is often clustered into chromocenters (Ceccarelli *et al.*, 1998; Fransz and de Jong, 2011). This type of nuclear organization was reliably described solely in plants. In most monocentric species, the maximum number of chromocenters corresponds to the chromosome number. Yet, the average number of chromocenters is always less than the chromosome number, indicating that the chromocenters of different chromosomes associate. This was demonstrated for *Arabidopsis thaliana* (0.435 Gbp/1C; Schmuths et al. 2004) where the chromocenters contain the majority of the genomic repeats, including transposons, the tandemly arrayed centromeric 180-bp repeat, and ribosomal genes (Fransz *et al.*, 2002). *Cucumis sativus* (0.882 Gbp/1C; Ramachandran and Narayan, 1985) nuclei also contain small heterochromatic chromocenters.

(ii) *Nicotiana tabacum* (5.072 Gbp/1C; Nagl *et al.*, 1983) and *Senecio viscosus* (1.519 Gbp/1C; Nagl *et al.*, 1983) nuclei contain numerous discrete complexes of condensed chromatin (chromomeres), which are scattered throughout the whole nucleoplasm.

(iii) *Hyacinthus orientalis* (20.874 Gbp/1C; Brandham and West, 1993; Nagl *et al.*, 1983) and *Allium flavum* (12.515 Gbp/1C; Baranyi and Greilhuber, 1999a; Nagl, 1985) nucleoplasm is filled with a meshwork of thick anastomosing fibers of condensed chromatin (chromonemata). To our knowledge, this type of heterochromatin organization was never described in animals, and this type of condensed interphase chromatin is scarcely studied.

Heterochromatin can be structurally reorganized during replication. As a general rule, replication leads to the decompaction of the condensed chromatin domains. For example, a transient heterochromatin decompaction associated with the processive DNA synthesis during replication was demonstrated in cultured human cells (Chagin *et al.*, 2019). Intuitively, the high amount of condensed chromatin in plant nuclei showing a chromonema organization might require a more robust reorganization of the nucleus, than typical for animal cells.

Here, we investigated the interphase nucleus organization in 32 plant species by transmission electron microscopy and found that in all giant-genome plants condensed chromatin forms thick threads (interphase chromonemata). Then, we studied chromatin reorganization during and after replication in root meristem nuclei of *Nigella damascena* with a large genome size of 10,584.0 Gbp/1C. We showed that about half of its genome is composed of tandem repeats (preferentially, LTR-retrotransposons). Condensed chromatin in *N. damascena* nuclei forms a typical chromonema meshwork. Super-resolution microscopy on semi-thin and ultra-thin sections revealed that replication induces chromonema decompaction, leading to the reorganization of the global nucleus morphology. Via correlative light and electron microscopy (CLEM) we showed that the replication occurs within decondensed diffuse chromatin, and that it is not accompanied by the formation of replication factories.

Materials and methods

Experimental objects

Seeds from 32 different species (Table 1) were cultivated for several days in a humidified chamber at 23°C protected from light. The majority of seeds were purchased from the Gavrish

Company (Russia). In the case of *Vicia* species, we re-analyzed images that were acquired previously in our laboratory, but the origin of these seeds is unknown.

Transmission electron microscopy (TEM)

Root tips were fixed in 2.5% glutaraldehyde in 100 mM cacodylate buffer, post-fixed in 1% OsO_4, dehydrated in ethanol and propylene oxide, and embedded in SPI-Pon 812 (SPI Supplies, US). The ultra-thin sections (~90 nm) were stained with uranyl acetate and lead citrate and examined using a JEM-1400 electron microscope (Jeol, Japan).

Replication labeling

Nigella damascena L. seeds were purchased from the Gavrish Company (cat. no. 002364; Russia). The seeds were grown in a Petri dish covered with filter paper at 25°C in the dark, and ~10 mm long sprouts were used for the study. For pulse labeling, the germinated seeds were incubated in 50 µM 5-ethynyl-2′-deoxyuridine (EdU; Invitrogen, USA) for 15 min (CLEM) or 30 min (light microscopy). In the case of chase labeling, EdU was then substituted with 200 µM thymidine for 30 min. Thymidine was subsequently removed and the sprouts were additionally cultivated for 1.5 hours in distilled water before fixation. In all experiments, the replication detection was carried out using the Click-iT EdU Cell Proliferation Kit for Imaging (AlexaFluor 555 dye; Invitrogen, USA) following the manufacturer's protocol.

Light microscopy

Ca. 1.0 mm long root tips were excised and fixed with 4% formaldehyde in 0.5-fold PBS for 2 h. After fixation, they were embedded in LR White resin (Sigma, USA). Semi-thin (~200 nm) sections were cut using an Ultratome LKB-III (LKB, Sweden). EdU was detected using a Click-iT EdU Alexa 555 Imaging Kit (Invitrogen, USA). DNA was stained with DAPI and mounted in Mowiol (Calbiochem, USA) containing the anti-bleaching agent DABCO (Sigma, USA). Sections were imaged using an Axiovert 200M microscope equipped with a Plan-Apochromat 100x/1.4 objective (Carl Zeiss GmbH) and a CCD camera (ORCAII-ERG2, Hamamatsu).

To analyze the ultrastructural organization of chromatin and replication beyond the classical Abbe–Rayleigh limit of ~250 nm, spatial structured illumination microscopy (3D-SIM) was performed to achieve a lateral resolution of ~140 nm (super-resolution, attained with a 561 nm laser). We used an Elyra PS.1 microscope system equipped with a Plan-Apochromat 63×/1.4 oil objective and the ZENBlack software (Carl Zeiss GmbH). Image stacks were captured separately for each fluorochrome using 405 nm (DAPI), and 561 nm (Alexa Fluor 555) laser lines for excitation and appropriate emission filters (Weisshart *et al.*, 2016; Kubalová *et al.*, 2021). Zoom-in sections are presented as single slices to detect the subnuclear chromatin structures at the super-resolution level.

Correlative light and electron microscopy (CLEM)

For correlative light and electron microscopy, we adopted a previously published protocol. After EdU labeling, root tips were fixed in 2.5% glutaraldehyde in 100 mM cacodylate buffer overnight, followed by a brief permeabilization in 0.1% Triton X-100 for 5 min. For EdU detection, the Click-iT EdU Cell Proliferation Kit for Imaging, AlexaFluor 555 dye (Invitrogen, US) was used, but the incubation in the reaction mixture was extended to 16 h. Then, the samples were embedded in SPI-Pon 812 resin as described above. Ultra-thin (~100 nm) sections were prepared using a Reichert-Jung Ultracut E ultramicrotome (Reichert, Germany) and mounted on single-slot grids with formvar support film. The sections were stained with 2µg/ml DAPI (ThermoScientific, USA) in 1×PBS, and then carefully mounted on a microscope slide under a coverslip in a water drop. The sections were photographed using a Nikon C2

microscope with a Plan-Apochromat 60x/1.4 oil objective. Then, the coverslips were removed, and the grids were stained with uranyl acetate and lead citrate and examined using a JEM-1400 electron microscope (Jeol, Japan).

To align the LM and EM images for CLEM analysis, we used a specifically developed image registration approach. First, we segmented the nucleus in both EM and LM images. For LM, we used the DAPI channel as the nucleus structure appears more prominent. Then, we upscaled the LM images to the same resolution as the EM images, from 1px = 63.4nm to 1px = 4.4nm. Since the LM images are quite smooth, such upscale did not introduce significant artifacts to the images.

The image registration was performed in two stages: coarse and fine. The coarse registration used the elasticity-based cell image registration approach described elsewhere. The method uses the nucleus mask as a reference and transforms the LM images to the EM images such that the nucleus masks are perfectly aligned. The transformation is constrained by the elasticity laws and corresponds to the nature of the actual nuclei motion. The fine stage was performed using an intensity-based approach. The condensed chromatin areas in DAPI were segmented and used as keypoints for the optimization-based image registration. We chose the thin-plate spline motion model with these keypoints as control points and mutual information as the cost function since the images are of different modalities. For both registration stages we applied equal transformation to the both channels of the LM images.

Since some deformations and distortions may occur during this double imaging process, we developed a special software for precise superpositioning of light and electron microscopy images. In round nuclei, the correction led to the almost perfect image overlap, but in elongated nuclei, we achieved only partial superposition. Therefore, we visually assessed the accuracy of alignment of condensed chromatin images in the TEM and DAPI images, and removed the regions with inaccurate alignment from the analysis.

DNA extraction and sequencing

Genomic DNA was extracted from the roots of *N. damascena* using the CTAB method. Library preparation followed the NEBNext Ultra II DNA Library Prep Kit for Illumina protocol (New England Biolabs, MA, US). Size selection of adapter-ligated DNA was performed as described in the protocol, and the average length of the DNA library fragments was ~400 bp. Genome sequencing was performed using the Illumina MiSeq system to obtain ~20 mln paired-end (2×301 bp) reads. The genome size (in bp) of *N. damascena* was calculated using the formula: $genome\ size = DNA\ content\ (pg) \times (0.978 \times 10^9)$. The DNA content of *N. damascena* was determined to be 10.5 pg/1C (https://cvalues.science.kew.org/), and the genome size was estimated to be 10.269 Gbp/1C. The coverage of the sequenced genome was calculated according to the following formula: $coverage = (number\ of\ reads \times read\ length) / 1C\ genome\ size$.

Repeat identification and annotation

Repetitive elements in the genome were analyzed using the graph-based clustering algorithm implemented in the RepeatExplorer2 pipeline. Raw DNA reads were uploaded to the Galaxy server with installed RepeatExplorer tools available at https://repeatexplorer-elixir.cerit-sc.cz. The quality of the sequencing reads was checked using FastQC installed on the server. The reads were trimmed to the length of 151 nucleotides and filtered by the quality of 95% of bases equal to or above the quality cutoff value of 10. The random sampling of 5 mln read pairs was conducted with RepeatExplorer utilities on the server. Paired-end read sequences were converted to FASTA format and interlaced into a single file. Only read pairs with no overlap were selected for the graph-based clustering analysis performed with the “RepeatExplorer2

clustering" tool. The automatic annotations of the discovered clusters of repetitive elements were manually corrected.

The consensus sequences of the integrase domain of Tekay LTR retrotransposon were extracted using the DANTE tool installed on the RepeatExplorer Galaxy server. Briefly, the contigs assembled for each cluster were extracted from the RepeatExplorer2 result archive using the utility 'Extract contigs from RepeatExplorer2 archive'. Then DANTE was used to annotate protein domains in transposable elements. The filtered GFF3 file produced by DANTE was subsequently used to obtain the consensus sequences of protein domains. Multiple sequence alignment of integrase domain nucleotide sequences was conducted using MAFFT (version 7) (Katoh *et al.*, 2019). The consensus sequence was obtained using the EMBOSS Cons tool (Madeira *et al.*, 2022).

Data availability

Raw DNA sequencing data were deposited in Sequence Read Archive (SRA) with accession number PRJNA939363.

Terminology

Sister chromatids of large (>12 Mb) chromosomes are formed by helically coiled chromatin threads during somatic and meiotic cell divisions (Baranetzky, 1880; Shinke, 1930; Manton, 1950; Kubalová *et al.*, 2023). Vejdovsky, 1912 named them 'chromonemata' (from Greek: chromo=color + nēma=thread; singular: chromonema). Later, the term 'chromonema' was also used to designate chromatin fibers in interphase nuclei of some plants (Sparvoli *et al.*, 1965). In this article, we use the term 'chromonema' in the second meaning (for discussion see also Kuznetsova and Sheval, 2016).

Results

Nuclear organization in plants depends on genome size

We analyzed the ultrastructural organization of root meristematic cells of 32 plant species and found, in agreement with published data (Nagl *et al.*, 1983; Nagl, 1985), three variants of nuclear organization. (i) In the first variant, the major part of the nucleoplasm volume was occupied by diffuse chromatin (euchromatin). Heterochromatin was rare and formed small blocks (chromocenters) preferentially in contact with the nuclear envelope (Fig. 1A). (ii) In the second variant, heterochromatin was more abundant and formed irregular-shaped complexes (chromomeres) not only in contact with the nuclear envelope but also throughout the nucleoplasm (Fig. 1B). (iii) In the third variant, nuclei were filled with a meshwork of thick (150-300 nm) heterochromatin fibers, which occupy roughly about half of all area of the nucleoplasm (Fig. 1C). Such heterochromatin fibers were described in the nuclei of some plants and were referred to as 'chromonemata' (Sparvoli *et al.*, 1965; Nagl and Fusenig, 1979; Kuznetsova and Sheval, 2016). In addition to the three typical nuclear variants shown in Figs. 1A-C transient variants were observed. But we did not find nuclei with a perinucleolar layer of heterochromatin, as typical for animals.

Analyzing the genome size of selected plants from the Plant DNA C-values Database, we found a strong correlation between genome size and nuclear organization (Fig. 1D). Plants showing variant 1 nuclei have relatively small genome sizes (<1.5 Gbp/1C) (Fig. 1D; Supplementary Fig. S2). Plants containing variant 2 nuclei present medium genome sizes (~1.5-5 Gbps) (Fig. 1D; Supplementary Fig. S3), and plants with chromonemata exhibit large genome sizes (>5 Gbps) (Fig. 1D; Supplementary Fig. S4). Thus, the chromonema organization of heterochromatin might be the consequence of extremely large genome sizes. Altogether, we conclude that the chromatin organization in plants depends on genome size.

Repetitive DNA represents more than half of the N. damascena genome

For a more detailed analysis of genome and nucleus organization in giant-genome plants, we analyzed *N. damascena*, which we had previously used to study mitotic chromosome organization (Kuznetsova *et al.*, 2017). To estimate the content of tandem repeats we performed DNA sequencing. After read trimming, random sampling, and filtering of non-overlapping read pairs 4,685,280 reads were left. These reads were used for graph-based clustering and repeat annotation via RepeatExplorer2. The repeat composition of the genome was inferred from 4,057,802 reads, which were randomly sampled and analyzed by the pipeline. About 58% of the reads belonged to 211 top clusters that were defined as those containing at least 405 reads (≥0.01% of analyzed reads). Automated cluster annotation was manually verified, and for three clusters the annotations were corrected. The final verified cluster annotation was used for repeat quantification. 15 clusters containing 27,581 reads were annotated as organellar (plastid and mitochondrial) sequences. The remaining 4,030,221 reads represented nuclear DNA and corresponded to ~0.06× coverage of the nuclear genome.

Circa 57% of the nuclear genome was composed of repetitive sequences, at which the repeatome was dominated by LTR-retrotransposons, representing ~50% of the genome (Fig. 2). The Tekay clade of chromoviral Ty3/Gypsy LTR-retrotransposons was the most abundant, comprising ~30% of the genome. Other abundant LTR families included Ty3/Gypsy Athila (8.16%) and Ty3/Gypsy Retand (2.11%). Unclassified LTR elements and unclassified repeats occupied 8.54% and 5.54%, respectively, of the genome. DNA transposons (class II), including MuDR_Mutator and EnSpm_CACTA families, contributed only to 0.44% of the genome. Satellite DNA and rDNA corresponded to 0.47% and 0.32% of the genome coverage, respectively.

Replication patterns in N. damascena

For replication labeling, we incubated living roots of *N. damascena* for 30 min with the 5-ethynyl-2′-deoxyuridine (EdU) which becomes detected by click-chemistry. To obtain a higher resolution and better signal-to-noise ratio in a light microscope, we used semi-thin (200-250 nm) root sections embedded in an acrylic medium.

We clearly distinguished three major replication patterns in *N. damascena* (Fig. 3A), which were substantially different from those in mammals (O'Keefe *et al.*, 1992). In animal nuclei, in early S-phase, the replication foci are distributed throughout the nucleoplasm (replication of euchromatin). In middle S-phase, discrete replication foci could be visible in contact with nucleoli and nuclear envelope (replication of facultative heterochromatin) and in late S-phase, a only few discrete foci persist (replication of constitutive heterochromatin). In *N. damascena*, we identified three major types of nuclei, differing by number and localization of EdU labels (replication patterns) (Fig. 3A). In type 1 nuclei, EdU labels discrete foci inside euchromatin. The type 2 nuclei were intensively labeled, and the labeled chromatin filled the major part of the nucleoplasm, excluding large blocks of condensed chromatin and nucleoli. The staining intensity in type 2 nuclei was substantially higher than in type 1 nuclei, allowing us to identify these patterns more reliably. In pattern 3, only a few discrete foci were visible. Compared to pattern 2 no analogous labeling was found in animals (O'Keefe *et al.*, 1992). It seems that these patterns in *N. damascena* were due to the chromonema structure, preventing the formation of perinucleolar and peripheral layers.

In all three replication patterns, EdU labeling colocalized with decondensed chromatin. However, it was not possible to distinguish whether eu- or heterochromatin was being replicated. Therefore, we additionally analyzed EdU labeling under chase conditions, i.e., fixation 2 h after pulse labeling, when replication of EdU-labeled regions was complete (Fig. 3B). In type 1 nuclei, the distribution of EdU-labeled regions was not significantly altered.

However, type 2 and 3 nuclei were significantly reorganized. EdU appeared within chromonemata (type 2) and within discrete chromatin blocks (type 3).

To clarify these visual observations, we used density profiles (Fig. 3C), which also show that after pulse labeling, EdU signals are located within the decondensed chromatin of all three types of nuclei. However, after chase labeling, the signals were located within decondensed chromatin in type 1 nuclei, but within condensed chromatin in type 2 and 3 nuclei. These data suggest that euchromatin replication occurred in type 1 nuclei, but heterochromatin replication occurred in type 2 and 3 nuclei. In addition, heterochromatin was found to decondense during replication and then re-condense.

Global heterochromatin decondensation during middle S-phase

As demonstrated above, heterochromatin was decompacted during replication and recompacted after replication. In type 2 nuclei, the heterochromatin decondensation seems to lead to chromonema decondensation inducing a global nucleus reorganization. Via DNA-specific DAPI labeling, thinner chromatin fibers became visible in addition to chromonemata (Fig. 3). Such nuclei can be identified by the absence of the regular meshwork of chromonemata. This allowed identifying type 2 nuclei only through DAPI labeling, without EdU staining.

To achieve more accurate visualization of this global chromatin reorganization during replication, we applied 3D-SIM on semi-thin (~200 nm) sections (Fig. 4). We performed both visual analysis and analysis of density profiles to reveal the colocalization between condensed chromatin and replication domains. In type 1 nuclei, the replication foci were visible within decondensed chromatin, preferentially near to either chromonemata or some non-numerous thinner (~100 nm) threads (Fig. 4A). In type 2 nuclei, we observed numerous thin (~100 nm) threads of condensed chromatin between interphase chromonemata, which, perhaps, correspond to decondensed regions of replicating chromonemata (Fig. 4B). The replication foci were located either near the surface of chromonemata or near thin threads of condensed chromatin, but were not overlapped. The largest replication foci were found near or in contact with these thin threads of condensed chromatin, i.e. with putative decondensed chromonemata. In type 3 nuclei, the replication foci were also located in decondensed chromatin. Using 3D-SIM, we were able to detect subunits inside large replication foci (compare Fig. 3A, bottom panels and Fig. 4C).

Thus, across the whole S-phase replicating DNA localizes predominantly outside but preferentially in contact with condensed chromatin. Some interchromatin regions were free of chromatin or replication foci. Because DAPI does not allow the detection of thin chromatin fibers for co-localization with replication foci we performed additional electron microscopy.

Ultrastructural organization of replicating chromonema

To investigate the ultrastructural organization of replicating chromatin, we combined fluorescence and electron microscopy (correlative light and electron microscopy, CLEM). We used a specifically developed two-stage non-rigid image registration approach to align the LM and EM images for the correlative analysis. The images were initially registered using the contour-based approach presented by (Sorokin *et al.*, 2018), followed by a keypoint-based registration with mutual information as the similarity metric.

The brightness of fluorescent images was substantially lower than that of semithin sections, therefore we were unable to analyze type 1 nuclei. Therefore, we used CLEM only for the analysis of heterochromatin decondensation during replication (type 2 nuclei) and reversed recompaction after replication (type 3 nuclei).

In the nucleoplasm of type 2 nuclei, some regions had a morphological organization typical for *N. damascena* nuclei (extended thick chromonemata), but other regions contained

numerous small (50-100 nm in diameter) discrete heterochromatin complexes of irregular shape overlapped with EdU labeling under pulse conditions (Fig. 5A). This indicates that these regions correspond to chromonema decondensation sites visible by light microscopy (compare Figs. 3A middle panels and Fig. 4B). At least partially, the EdU labels overlapped with heterochromatin (Fig. 5A). Under chase conditions, the heterochromatin was preferentially organized into thick threads (chromonemata), and the EdU labels preferentially overlapped with heterochromatin (Fig. 5B).

After measuring the overall colocalization of replication masks with condensed chromatin we found that the overlapping was enhanced under chase compared to pulse conditions (Fig. 5C). However, the fluorescent masks had a relatively low resolution due to diffraction. Therefore, we additionally calculated centroids of replication spots, assuming that these spots represent the actual replicating chromatin (replication forks) (cyan dots in Figs. 5A and B). We estimated the centroid positions relative to the border between heterochromatin and the interchromatin compartment. The replication centroids were preferentially located in the interchromosomal compartment under pulse conditions, and in heterochromatin under chase conditions (Fig. 5D).

A similar relocation of labeled chromatin was visible in type 3 nuclei. The EdU pulse labels appeared preferentially within decondensed chromatin, but also overlapped with condensed chromatin in the chase experiments.

Additionally, we analyzed the general organization of nuclei with typical and reorganized chromatin morphology in TEM images. We found that in all type 2 and 3 nuclei after impulse and chase chromatin labeling ~45% of the nucleoplasm area was occupied by condensed chromatin. Consequently, we conclude that replication in middle S-phase requires a significant chromonemata disassembly, but it seems that the amount of decondensed chromatin is minor during this process.

Discussion

The profound genome size variation between species was described in different groups of plants and animals, which occurred due to the expansion of different non-coding DNA sequences (Gregory, 2005). In some groups of animals and plants, a dramatic and yet inexplicable increase in genome size occurred. Plants with a giant genome are of particular interest, since an excess of DNA can lead to changes in the organization of interphase nuclei and mitotic chromosomes. Already in the earliest TEM work on plant chromatin ultrastructure, it was shown that networks of thick heterochromatin threads were present in interphase nuclei of *Tradescantia paludosa*, and these threads were referred to as ‘chromonemata’ (Sparvoli *et al.*, 1965). Additionally, we have previously shown that the chromosomes of plants with a large genome are arranged differently than those of plants with a small genome (Kuznetsova *et al.*, 2017).

The data of the present work indicate that genome increase changes the interphase nuclei morphology of plants by increasing the amount of condensed chromatin and changing its localization. We found that three previously found variants of plant nuclei (Nagl *et al.*, 1983) correspond to plant nuclei with small, large, and giant genomes, respectively.

To our knowledge, interphase chromonemata were not described in animals and may be specific for plants. For a more detailed investigation, we selected *N. damascena*, a plant with a giant genome (Olszewska and Osiecka, 1983) whose meristematic nuclei of roots show typical chromonemata, containing tandem repeats representing >50% of the global genome.

In cultured mammalian cells, heterochromatin can undergo cycles of decompaction-compaction during replication (Chagin *et al.*, 2019). Whether the chromonema forming chromatin in plant nuclei with a giant genome proceeds similar cycles, and whether this process

induces a significant global chromatin rearrangement in nuclei with heterochromatin overabundance was still unknown, but was now proven via our investigations.

Previously, we applied EdU incorporation on semi-thin root sections embedded in acrylic resin to identify replicating and post replicating chromatin (Kuznetsova *et al.*, 2017; Sheval, 2018). This method allows examining thin specimen slices (100-250 nm), with 2-3 times better axial (*z*) resolution than is achievable by wide-field fluorescence and confocal microscopy. We used conventional wide-field fluorescence microscopy for a general characterization of the labeling patterns. As a result, we identified three replication patterns, which, probably, correspond to (i) replication of decondensed chromatin (euchromatin; type 1), (ii) replication of condensed chromatin within chromosomes (type 2), and (iii) replication of discrete complexes of condensed chromatin (type 3). These patterns were slightly different from those described in animals. For example, we did not find nuclei in which replication foci were concentrated around nucleoli and at the nuclear periphery (a pattern typical for middle S-phase in animals). Apparently, this was due to the homogeneous heterochromatin distribution within the entire *N. damascena* nucleus. The abundant amount of heterochromatin may also explain the high labeling intensity within these nuclei. By analogy with animal cells, one can assume that the replication types 1, 2, and 3 may correspond to early, middle, and late S-phase, respectively.

In all three patterns, the replicating chromatin was predominantly diffuse, but after replication in type 2 and 3 nuclei (i.e., in the chase experiment), the labels were detected within condensed chromatin (in the case of pattern 2, as part of chromonemata). Thus, heterochromatin was decondensed during replication, and recondensed after replication. Additionally, we found that chromonemata replication led to the global reorganization of nuclei, detectable also by DAPI staining.

To characterize the organization of the replicating chromonemata (type 2 nuclei), we applied super-resolution 3D-SIM and CLEM microscopy, allowing us to detect the ultrastructural organization of chromatin. 3D-SIM showed that the replicating chromatin dispersed by decondensation locates close to the chromonemata. CLEM confirmed these observations. During replication, the replicating chromatin is predominantly dispersed outside of the condensed chromatin. After replication (chase conditions), the labels were localized almost entirely within the chromonemata (type 2 nuclei) or blocks of condensed chromatin (type 3 nuclei). The infrequent labeling of heterochromatin complexes in pulse experiments might be the result of the fast recondensation of chromatin after replication. To enhance the labeling intensity, we incubated the roots in EdU for a relatively long time of 30 min.

Surprisingly, by analyzing the overall effect of chromatin decondensation we found that the proportion of the area of condensed chromatin did not change. Thus, we assume that the chromatin decondensation affects at each time point only a relatively small fraction of the genome. As a result, we do not observe significant changes in the amount of condensed chromatin.

In short, we conclude that the replication of chromatin forming chromonemata in plant nuclei with a giant genome is accompanied by a similar decompaction-compaction cycle as described for animals. However, the abundance of such chromatin leads to a robust nuclear morphology reorganization not present in animals or in plants with small genomes.

Acknowledgment

We are grateful to A.V. Lazarev for technical support, D.O. Omelchenko and A.A. Penin for consultation and help with DNA isolation. This work was supported by the Russian Foundation for Basic Research (20-54-12016) and the Deutsche Forschungsgemeinschaft (Schu 762/11-1).

Table 1. Genome size (references from https://cvalues.science.kew.org/search) and heterochromatin organization in plants, evaluated in this study using TEM (Supplementary Figs. S1, S2 and S3).

Species	**Genome size (Gbp/1C)**	**Reference**	**Heterochromatin organization**
Daucus carota	0.461	(Nowicka *et al.*, 2016)	chromocenters
Brassica rapa	0.528	(Johnston *et al.*, 2005)	chromocenters
Cucurbita pepo	0.529	(Arumuganathan and Earle, 1991)	chromocenters
Linum usitatissimum	0.544	(Marie and Brown, 1993)	chromocenters
Brassica oleracea	0.671	(Arumuganathan and Earle, 1991)	chromocenters
Phaseolus vulgaris	0.701	(Marie and Brown, 1993)	chromocenters
Catharanthus roseus	0.784	(Zonneveld *et al.*, 2005)	chromocenters
Lupinus polyphyllus	0.784	(Kubešová *et al.*, 2010)	chromocenters
Cucumis sativus	0.882	(Ramachandran and Narayan, 1985)	chromocenters
Lycopersicon esculentum	0.980	(Obermayer *et al.*, 2002)	chromocenters
Gossypium herbaceum	1.671	(Hendrix and Stewart, 2005)	chromomeres
Vicia sativa	1.911	(Zonneveld *et al.*, 2005)	chromomeres
Dahlia variabilis	2.024	(Temsch *et al.*, 2008)	chromomeres

Zea mays	2.328	(Arumuganathan and Earle, 1991)	chromomeres
Rudbeckia hirta	3.479	(Bai *et al.*, 2012)	chromomeres
Helianthus annuus	3.597	(Sanchez *et al.*, 2014)	chromomeres
Pisum sativum	4.263	(Zonneveld *et al.*, 2005)	chromomeres
Vicia cracca	5.586	(Grime and Mowforth, 1982)	chromomeres
Vicia sepium	4.606	(Rees *et al.*, 1966)	chromonemata
Hordeum vulgare	5.189	(Jakob *et al.*, 2004)	chromonemata
Lathyrus gorgoni	6.370	(Nandini *et al.*, 1997)	chromonemata
Lathyrus odoratus	8.036	(Murray *et al.*, 1992)	chromonemata
Lathyrus latifolius	8.389	(Pustahija *et al.*, 2013)	chromonemata
Nigella sativa	10.388	(Bennett and Smith, 1976)	chromonemata
Nigella damascena	10.584	(Olszewska and Osiecka, 1983)	chromonemata
Allium fistulosum	11.642	(Baranyi and Greilhuber, 1999b)	chromonemata
Vicia faba	13.348	(Kron and Husband, 2012)	chromonemata
Allium altaicum	15.190	Ohri et al.,1996	chromonemata
Allium schoenoprasum	16.023	(Zonneveld *et al.*, 2005)	chromonemata
Allium cepa	16.508	(Barow and Meister, 2003)	chromonemata

Allium porrum	28.371	(Zonneveld *et al.*, 2005)	chromonemata
Allium ramosum	30.772	(Ohri *et al.*, 1998)	chromonemata

Figures

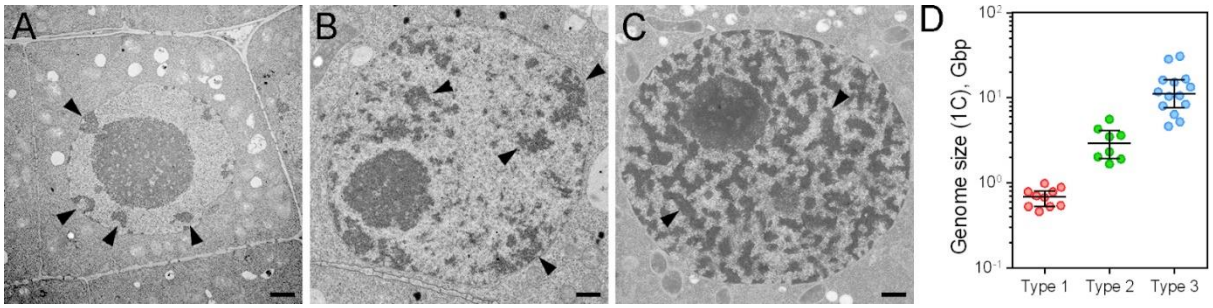

Fig. 1. Three variants of chromatin organization in root meristem nuclei of different plants. (A) Nucleus of *L. esculentum* (variant 1 nucleus). Heterochromatin forms only a few discrete complexes (chromocenters), which are located mainly on the periphery of the nucleus in contact with the nuclear envelope. (B) Nucleus of *D. variabilis* (variant 2 nucleus). Heterochromatin forms numerous complexes (chromomeres), very heterogeneous in structure and size, which are localized at the nuclear periphery, but also internally. (C) Nucleus of *N. Damascena* (variant 3 nucleus). Heterochromatin forms thick branching threads (chromonemata) filling the entire nucleoplasm. No predominant localization of heterochromatin at the nuclear periphery or around the nucleolus was identified. (D) The variant of nucleus organization is related to the genome size.
Detailed data are given in Table 1. For each variant of nucleus, the median and interquartile range are shown.

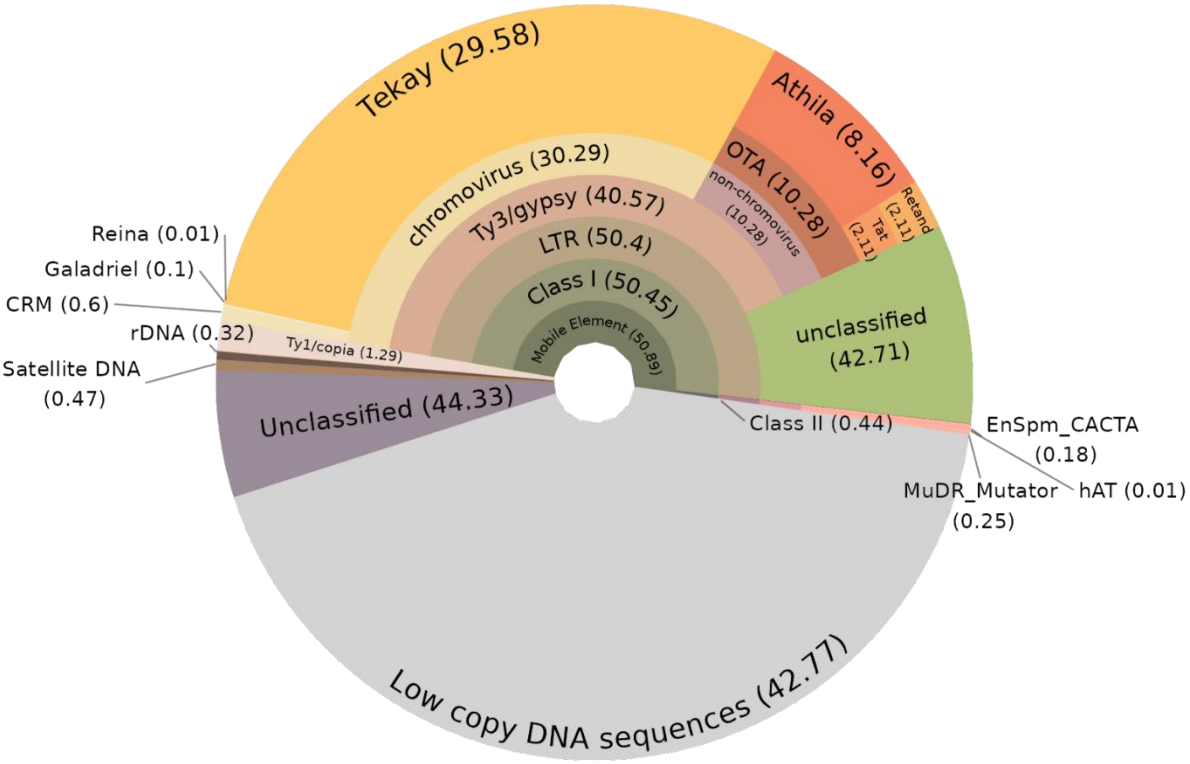

Fig. 2. Types of highly and moderately repeated DNA sequences in the *N. damascena* genome. The proportion of each repeat type or family is shown inside the parentheses. Repeat proportions were calculated by annotating clusters representing at least 0.01% of the genome in RepeatExplorer. For mobile elements, the members of each repeat family are indicated in the outer layers.

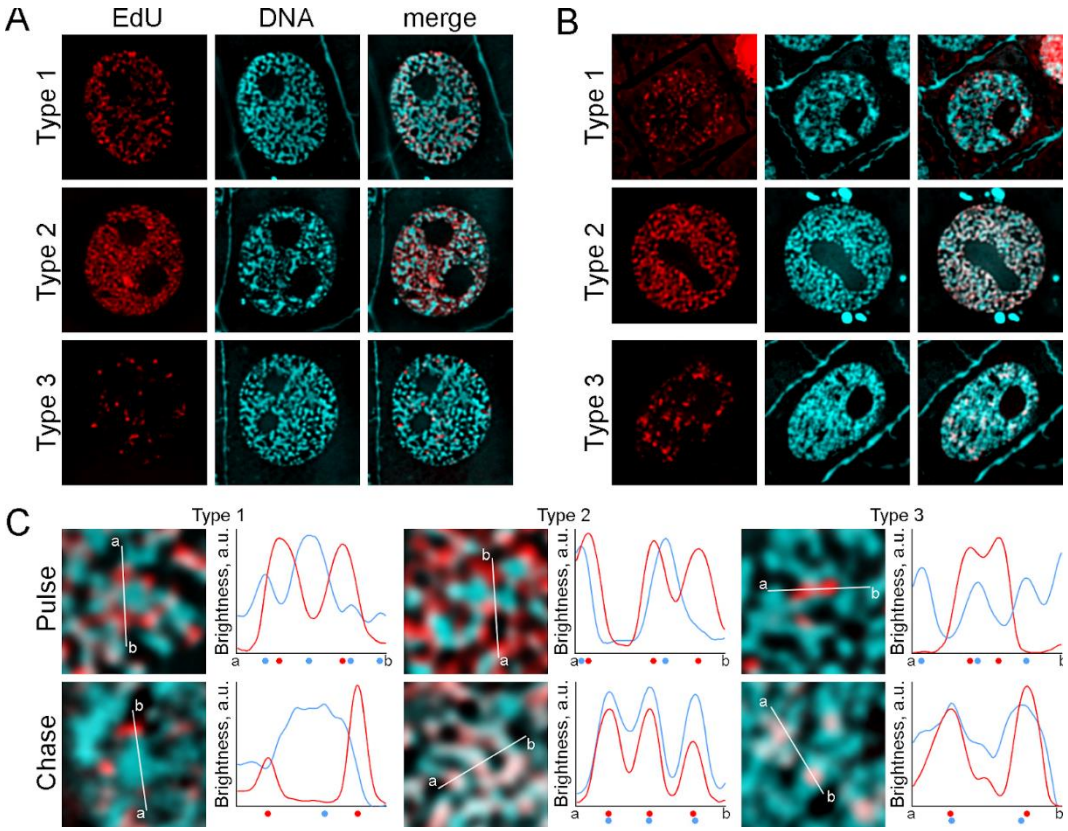

Fig. 3. Chromatin replication patterns in meristematic nuclei of *N. damascena*. (A) Three labeling types were classified under pulse conditions (labeling of chromatin during replication). For the acquisition of type 1 nuclei images, a 2-3 times higher exposure time was applied, required due to lower fluorescence intensity (see Supplementary Fig. S). The chromonema organization was partially disassembled in type 2 nuclei. (B) Three labeling types were classified under chase conditions (labeling of chromatin 2h after pulse labeling). The chromonemata in type 1 nuclei were decondensed, possibly because they were in middle S-phase. As well, under chase conditions, type 3 nuclei had different structure, possibly because they were in preprophase or even prophase (see Supplementary Fig. S). (C) Localization of replication foci (replicating chromatin) relative to chromonemata (heterochromatin) in all three nuclei types under pulse and chase conditions. Under pulse conditions the replicating chromatin is located always close to heterochromatin. Under chase conditions, the EdU labels were located similarly at the chromonemata surface in type 1 nuclei, or within the heterochromatin in type 2 and 3 nuclei. the dots under the density graphs indicate the positions of the maxima of heterochromatin (cyan dots) and EdU-containing chromatin (red dots).

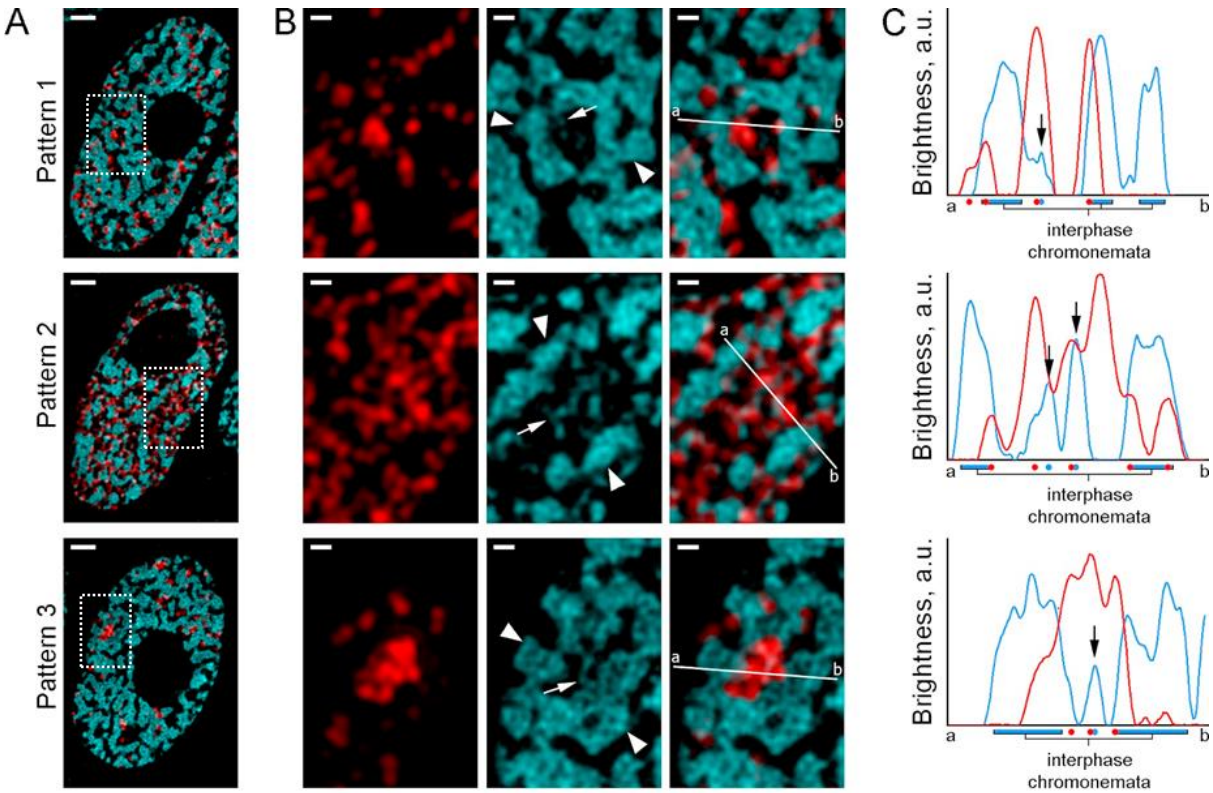

Fig. 4. Super-resolution (3D-SIM) microscopy of *N. damascena* nuclei during replication. **A** - general view of representative nuclei of type 1, 2 and 3 (top, middle and bottom panels, respectively). **B** - fragments of the nuclei from panels **A**. Chromonemata are marked by white arrowheads, thin threads of condensed chromatin - by white arrows. **C** - plot profiles through the a-b lines in panel B. The replicating chromatin (indicated by red dots under plots) in all cases is located at the boundary of thick threads of condensed chromatin (interphase chromonemata), but usually near thin threads of condensed chromatin (these threads are marked by blue dots under plots, and additionally indicated by black arrows in plots).

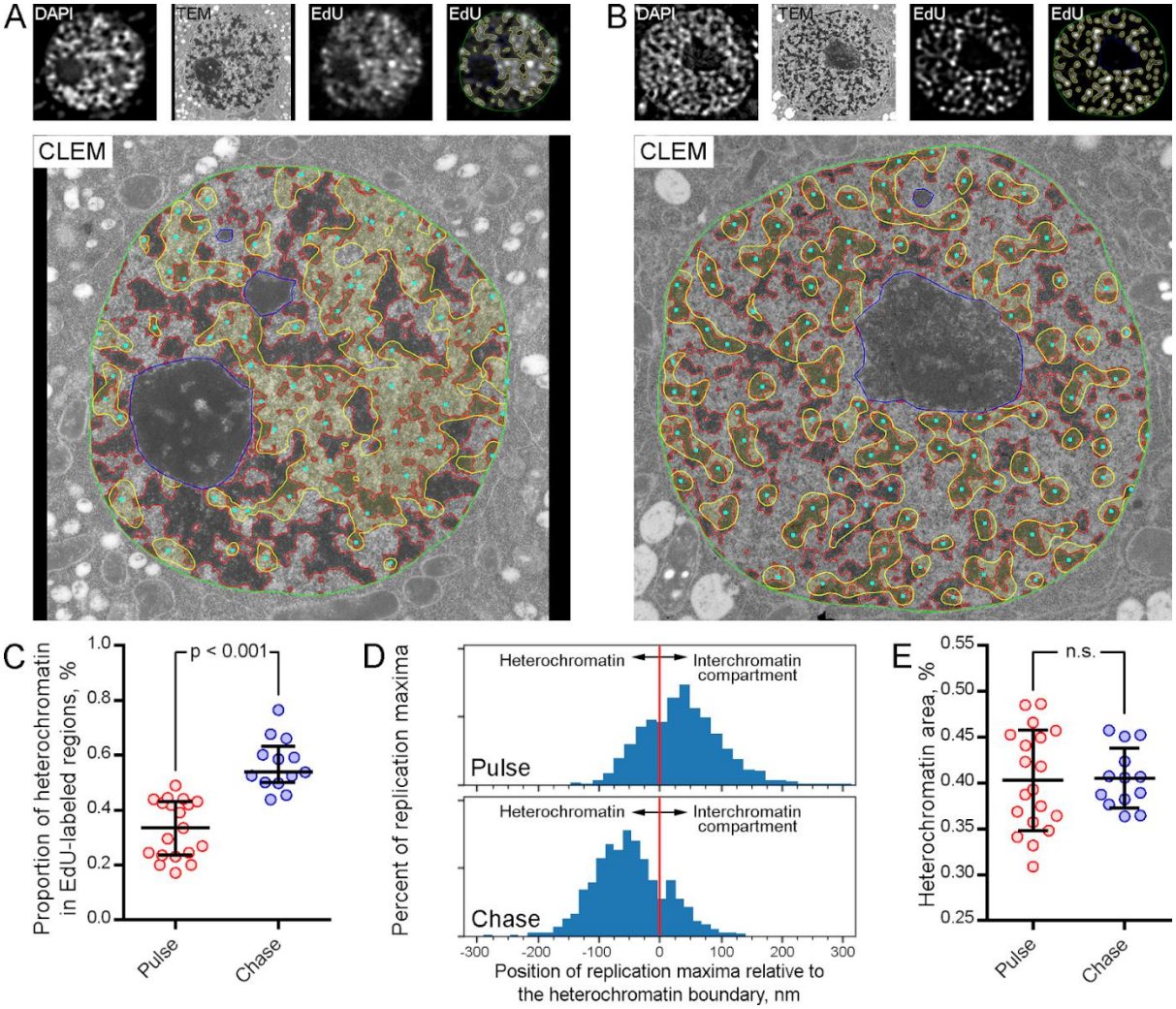

Fig. 5. Correlative light and electron microscopy (CLEM) of replicating chromatin in *N. damascena* nuclei (type 2 nuclei). (**A**) CLEM of a representative nucleus labeled with EdU under pulse conditions (labeling of just replicating chromatin). Top panel - images, which were used for the segmentation of nuclear structures, bottom panel - the result of segmentation (blue lines - non-chromatin structures, red lines - heterochromatin, yellow lines and filling - replication complexes, cyan dots - centroids of replication complexes). The replication complexes overlap preferentially with the interchromatin compartment, inside which small heterochromatin complexes are visible. (**B**) CLEM of a representative nucleus labeled with EdU under chase conditions (labeling of chromatin, whose replication was finished before fixation). Top panels - images, which were used for the segmentation of nuclear structures, bottom panel - the result of segmentation (color markings as in **A**). The replication complexes overlap preferentially with heterochromatin, which forms extended chromonemata. (**C**) Estimation of the overlap between replication complexes and heterochromatin. The proportion of the area of regions labeled with EdU, occupied by heterochromatin, is larger under chase than pulse conditions. The comparison was performed using the Mann–Whitney U test. (**D**) The localization of replication complex centroids relative to heterochromatin borders. Under pulse conditions, the majority of centroids (%) localized in the interchromatin compartments, but under chase conditions, the majority located inside heterochromatin. (**E**) Estimation of heterochromatin content in nuclei during and after replication of chromonemata (pulse and chase labeling of type 2 nuclei). The comparison was performed using the Mann–Whitney U test (n.s. – not significant).

References

Arifulin, E.A. (2015) Ultrastructural organization of replicating chromatin in prematurely condensed chromosomes. *Biopolym. Cell*, **31**, 249–254.

Arumuganathan, K. and Earle, E.D. (1991) Nuclear DNA content of some important plant species. *Plant Mol. Biol. Rep.*, **9**, 208–218.

Bai, C., Alverson, W.S., Follansbee, A. and Waller, D.M. (2012) New reports of nuclear DNA content for 407 vascular plant taxa from the United States. *Ann. Bot.*, **110**, 1623–1629.

Baranetzky, J. (1880) Die Kernteilung in den Pollenmutterzellen einiger Tradescantien. *Bot. Zeitschr.*, **38**, 281–296.

Baranyi, M. and Greilhuber, J. (1999a) Genome Size in Allium: In Quest of Reproducible Data. *Ann. Bot.*, **83**, 687–695.

Baranyi, M. and Greilhuber, J. (1999b) Genome size in *Allium*: In quest of reproducible data. *Ann. Bot.*, **83**, 687–695.

Barow, M. and Meister, A. (2003) Endopolyploidy in seed plants is differently correlated to systematics, organ, life strategy and genome size. *Plant Cell Environ.*, **26**, 571–584.

Belmont, A.S. and Bruce, K. (1994) Visualization of G1 chromosomes: a folded, twisted, supercoiled chromonema model of interphase chromatid structure. *J. Cell Biol.*, **127**, 287–302.

Bennett, M.D. and Smith, J.B. (1976) Nuclear dna amounts in angiosperms. *Philos. Trans. R. Soc. Lond. B Biol. Sci.*, **274**, 227–274.

Beseda, T., Cápal, P., Kubalová, I., Schubert, V., Doležel, J. and Šimková, H. (2020) Mitotic chromosome organization: General rules meet species-specific variability. *Comput. Struct. Biotechnol. J.*, **18**, 1311–1319.

Brandham, P.E. and West, J.P. (1993) Correlation between nuclear DNA values and differing optimal ploidy levels inNarcissus, Hyacinthus andTulipa cultivars. *Genetica*, **90**, 1–8.

Câmara AS, Kubalová I, Schubert V (in revision) Helical chromonema coiling is conserved in eukaryotes. Plant J

Ceccarelli, M., Morosi, L. and Cionini, P.G. (1998) Chromocenter association in plant cell nuclei: determinants, functional significance, and evolutionary implications. *Genome*, **41**, 96–103.

Chagin, V.O., Reinhart, B., Becker, A., Mortusewicz, O., Jost, K.L., Rapp, A., Leonhardt, H. and Cardoso, M.C. (2019) Processive DNA synthesis is associated with localized decompaction of constitutive heterochromatin at the sites of DNA replication and repair. *Nucleus*, **10**, 231–253.

Dong, P., Tu, X., Chu, P.-Y., Lü, P., Zhu, N., Grierson, D., Du, B., Li, P. and Zhong, S. (2017) 3D Chromatin Architecture of Large Plant Genomes Determined by Local A/B Compartments. *Mol. Plant*, **10**, 1497–1509.

Doyle, J.J. and Doyle, J.L. (1987) A rapid DNA isolation procedure for small quantities of fresh leaf tissue. *PHYTOCHEMICAL BULLETIN*. Available at: https://worldveg.tind.io/record/33886/ [Accessed March 14, 2023].

Eltsov, M., Maclellan, K.M., Maeshima, K., Frangakis, A.S. and Dubochet, J. (2008) Analysis of cryo-electron microscopy images does not support the existence of 30-nm chromatin fibers in mitotic chromosomes in situ. *Proc. Natl. Acad. Sci. U. S. A.*, **105**, 19732–19737.

Falk, M., Feodorova, Y., Naumova, N., et al. (2019) Heterochromatin drives compartmentalization of inverted and conventional nuclei. *Nature*, **570**, 395–399.

Feodorova, Y., Falk, M., Mirny, L.A. and Solovei, I. (2020) Viewing Nuclear Architecture through the Eyes of Nocturnal Mammals. *Trends Cell Biol.*, **30**, 276–289.

Finch, J.T. and Klug, A. (1976) Solenoidal model for superstructure in chromatin. *Proc. Natl. Acad. Sci. U. S. A.*, **73**, 1897–1901.

Fleischmann, A., Michael, T.P., Rivadavia, F., Sousa, A., Wang, W., Temsch, E.M., Greilhuber, J., Müller, K.F. and Heubl, G. (2014) Evolution of genome size and chromosome number in the carnivorous plant genus Genlisea (Lentibulariaceae), with a new estimate of the minimum genome size in angiosperms. *Ann. Bot.*, **114**, 1651–1663.

Fransz, P., De Jong, J.H., Lysak, M., Castiglione, M.R. and Schubert, I. (2002) Interphase chromosomes in Arabidopsis are organized as well defined chromocenters from which euchromatin loops emanate. *Proc. Natl. Acad. Sci. U. S. A.*, **99**, 14584–14589.

Fransz P, de Jong H. (2011) From nucleosome to chromosome: a dynamic organization of genetic information. *Plant J.*, **66**, 4–17.

Gregory, T.R. (2005) The C-value enigma in plants and animals: a review of parallels and an appeal for partnership. *Ann. Bot.*, **95**, 133–146.

Gregory, T. R. (2011) The Evolution of the Genome, Elsevier. https://doi.org/10.1016/B978-0-12-301463-4.X5000-1

Grime, J.P. and Mowforth, M.A. (1982) Variation in genome size—an ecological interpretation. *Nature*, **299**, 151–153. Available at: [Accessed February 17, 2023].

Hendrix, B. and Stewart, J.M. (2005) Estimation of the nuclear DNA content of gossypium species. *Ann. Bot.*, **95**, 789–797.

Jakob, S.S., Meister, A. and Blattner, F.R. (2004) The considerable genome size variation of Hordeum species (Poaceae) is linked to phylogeny, life form, ecology, and speciation rates. *Mol. Biol. Evol.*, **21**, 860–869.

Johnston, J.S., Pepper, A.E., Hall, A.E., Chen, Z.J., Hodnett, G., Drabek, J., Lopez, R. and Price, H.J. (2005) Evolution of genome size in Brassicaceae. *Ann. Bot.*, **95**, 229–235.

Kapusta, A., Suh, A. and Feschotte, C. (2017) Dynamics of genome size evolution in birds and mammals. *Proc. Natl. Acad. Sci. U. S. A.*, **114**, E1460–E1469.

Katoh, K., Rozewicki, J. and Yamada, K.D. (2019) MAFFT online service: multiple sequence alignment, interactive sequence choice and visualization. *Brief. Bioinform.*, **20**, 1160–1166.

Kireeva, N., Lakonishok, M., Kireev, I., Hirano, T. and Belmont, A.S. (2004) Visualization of early chromosome condensation: a hierarchical folding, axial glue model of chromosome structure. *J. Cell Biol.*, **166**, 775–785.

Kornberg, R.D. (1974) Chromatin structure: a repeating unit of histones and DNA. *Science*, **184**, 868–871.

Kron, P. and Husband, B.C. (2012) Using flow cytometry to estimate pollen DNA content: improved methodology and applications. *Ann. Bot.*, **110**, 1067–1078.

Kubalová, I., Câmara, A.S., Cápal, P., et al. (2023) Helical coiling of metaphase chromatids. *Nucleic Acids Res.*, **51**, 2641–2654.

Kubalová, I., Němečková, A., Weisshart, K., Hřibová, E. and Schubert, V. (2021) Comparing Super-Resolution Microscopy Techniques to Analyze Chromosomes. *Int. J. Mol. Sci.*, **22**. Available at: http://dx.doi.org/10.3390/ijms22041903.

Kubešová, M., Moravcova, L., Suda, J., Jarošík, V. and Pyšek, P. (2010) Naturalized plants have smaller genomes than their non-invading relatives: a flow cytometric analysis of the Czech alien flora. *Preslia*. Available at: https://www.researchgate.net/profile/Petr-Pysek/publication/287688630_Naturalized_plants_have_smaller_genomes_than_their_non-invading_relatives_A_flow_cytometric_analysis_of_the_Czech_alien_flora/links/5970cdcc458515fa8de6e39e/Naturalized-plants-have-smaller-genomes-than-their-non-invading-relatives-A-flow-cytometric-analysis-of-the-Czech-alien-flora.pdf.

Kuznetsova, M.A., Chaban, I.A. and Sheval, E.V. (2017) Visualization of chromosome condensation in plants with large chromosomes. *BMC Plant Biol.*, **17**, 153.

Kuznetsova, M.A. and Sheval, E.V. (2016) Chromatin fibers: from classical descriptions to modern interpretation. *Cell Biol. Int.*, **40**, 1140–1151.

Lee, S.-I. and Kim, N.-S. (2014) Transposable elements and genome size variations in plants. *Genomics Inform.*, **12**, 87–97.

Leitch IJ, Johnston E, Pellicer J, Hidalgo O, Bennett MD. 2019. Plant DNA C-values database (release 7.1, Apr 2019) https://cvalues.science.kew.org/

Leitch, I.J., Hanson, L., Lim, K.Y., Kovarik, A., Chase, M.W., Clarkson, J.J. and Leitch, A.R. (2008) The ups and downs of genome size evolution in polyploid species of Nicotiana (Solanaceae). *Ann. Bot.*, **101**, 805–814.

Lieberman-Aiden, E., Berkum, N.L. van, Williams, L., et al. (2009) Comprehensive mapping of long-range interactions reveals folding principles of the human genome. *Science*, **326**, 289–293.

Li, Z., McKibben, M.T.W., Finch, G.S., Blischak, P.D., Sutherland, B.L. and Barker, M.S. (2021) Patterns and Processes of Diploidization in Land Plants. *Annu. Rev. Plant Biol.*, **72**, 387–410.

Madeira, F., Pearce, M., Tivey, A.R.N., Basutkar, P., Lee, J., Edbali, O., Madhusoodanan, N., Kolesnikov, A. and Lopez, R. (2022) Search and sequence analysis tools services from EMBL-EBI in 2022. *Nucleic Acids Res.*, **50**, W276–9.

Maeshima, K., Imai, R., Tamura, S. and Nozaki, T. (2014) Chromatin as dynamic 10-nm fibers. *Chromosoma*, **123**, 225–237.

Manton, I. (1950) The spiral structure of chromosomes. *Biol. Rev. Camb. Philos. Soc.*, **25**, 486–508.

Marie, D. and Brown, S.C. (1993) A cytometric exercise in plant DNA histograms, with 2C values for 70 species. *Biol. Cell*, **78**, 41–51.

Marsden, M.P. and Laemmli, U.K. (1979) Metaphase chromosome structure: evidence for a radial loop model. *Cell*, **17**, 849–858.

McDowall, A.W., Smith, J.M. and Dubochet, J. (1986) Cryo-electron microscopy of vitrified chromosomes in situ. *EMBO J.*, **5**, 1395–1402.

Michael, T.P. (2014) Plant genome size variation: bloating and purging DNA. *Brief. Funct. Genomics*, **13**, 308–317.

Murray, B.G., Hammett, K.R.W. and Standring, L.S. (1992) Genomic constancy during the development of Lathyrus odoratus cultivars. *Heredity* , **68**, 321–327. Available at: [Accessed April 12, 2023].

Nagl, W. (1985) Chromatin organization and the control of gene activity. *Int. Rev. Cytol.*, **94**, 21–56.

Nagl, W. and Bachmann, K. (1980) Condensed chromatin in diploid and allopolyploid microseris species with different genome size: a quantitative electron microscopic study. *Theor. Appl. Genet.*, **57**, 107–111.

Nagl, W. and Fusenig, H.-P. (1979) Types of Chromatin Organization in Plant Nuclei. In W. Nagl, V. Hemleben, and F. Ehrendorfer, eds. *Genome and Chromatin: Organization, Evolution, Function: Symposium, Kaiserslautern, October 13–15, 1978*. Vienna: Springer Vienna, pp. 221–233.

Nagl, W., Jeanjour, M. and Kling, H. (1983) GENOME AND CHROMATIN ORGANIZATION IN HIGHER-PLANTS. *Biol. Zent. Bl.*

Nandini, A.V., Murray, B.G., O'brien, I.E.W. and Hammett, K.R.W. (1997) Intra- and interspecific variation in genome size in Lathyrus (Leguminosae). *Bot. J. Linn. Soc.*, **125**, 359–366.

Novák, P., Neumann, P. and Macas, J. (2020) Global analysis of repetitive DNA from unassembled sequence reads using RepeatExplorer2. *Nat. Protoc.*, **15**, 3745–3776.

Nowicka, A., Sliwinska, E., Grzebelus, D., Baranski, R., Simon, P.W., Nothnagel, T. and Grzebelus, E. (2016) Nuclear DNA content variation within the genus Daucus (Apiaceae) determined by flow cytometry. *Sci. Hortic.* , **209**, 132–138.

Obermayer, R., Leitch, I.J., Hanson, L. and Bennett, M.D. (2002) Nuclear DNA C-values in 30 species double the familial representation in pteridophytes. *Ann. Bot.*, **90**, 209–217.

Ohri, D., Fritsch, R.M. and Hanelt, P. (1998) Evolution of genome size inAllium (Alliaceae). *Osterr. bot. Z.*, **210**, 57–86.

O'Keefe, R.T., Henderson, S.C. and Spector, D.L. (1992) Dynamic organization of DNA replication in mammalian cell nuclei: spatially and temporally defined replication of chromosome-specific alpha-satellite DNA sequences. *J. Cell Biol.*, **116**, 1095–1110.

Olins, A.L. and Olins, D.E. (1974) Spheroid chromatin units (v bodies). *Science*, **183**, 330–332.

Olszewska, M.J. and Osiecka, R. (1983) The rlationship between 2 C DNA content, life cycle type, systematic position and the dynamics of DNA endoreplication in parenchyma nuclei during growth and differentiation of roots in some dicotyledonous herbaceous species. *Biochemie und Physiologie der Pflanzen*, **178**, 581–599. Available at: http://dx.doi.org/10.1016/s0015-3796(83)80073-0.

Pellicer, J., Fay, M.F. and Leitch, I.J. (2010) The largest eukaryotic genome of them all? *Bot. J. Linn. Soc.*, **164**, 10–15. Available at: [Accessed March 19, 2023].

Pellicer, J. and Leitch, I.J. (2020) The Plant DNA C-values database (release 7.1): an updated online repository of plant genome size data for comparative studies. *New Phytol.*, **226**, 301–305.

Pustahija, F., Brown, S.C., Bogunić, F., et al. (2013) Small genomes dominate in plants growing on serpentine soils in West Balkans, an exhaustive study of 8 habitats covering 308 taxa. *Plant Soil*, **373**, 427–453.

Ramachandran, C. and Narayan, R.K. (1985) Chromosomal DNA variation in *Cucumis*. *Theor. Appl. Genet.*, **69**, 497–502.

Redi, C.A. and Capanna, E. (2012) Genome size evolution: sizing mammalian genomes. *Cytogenet. Genome Res.*, **137**, 97–112.

Rees, H., Cameron, F.M., Hazarika, M.H. and Jones, G.H. (1966) Nuclear variation between diploid angiosperms. *Nature*, **211**, 828–830.

Sanchez, P.L., Costich, D.E., Friebe, B., Coffelt, T.A., Jenks, M.A. and Gore, M.A. (2014) Genome size variation in guayule and mariola: Fundamental descriptors for polyploid plant taxa. *Ind. Crops Prod.*, **54**, 1–5.

Schmuths H, Meister A, Horres R, Bachmann K. Genome size variation among accessions of Arabidopsis thaliana. Ann Bot. 2004 Mar;93(3):317-21

Schubert, V., Berr, A. and Meister, A. (2012) Interphase chromatin organisation in Arabidopsis nuclei: constraints versus randomness. *Chromosoma*, **121**, 369–387.

Sheval, E.V. (2018) Analysis of chromosome condensation/decondensation during mitosis by EdU incorporation in *Nigella damascena* L. seedling roots. *Bio-protocol*, **8**, e2726.

Shinke, N. (1930) On the spiral structure of chromosomes in some higher plants. *Memoirs of the College of Science, Kyoto Imperial University. Ser. B*, **5**, 239–245.

Solovei, I., Kreysing, M., Lanctôt, C., Kösem, S., Peichl, L., Cremer, T., Guck, J. and Joffe, B. (2009) Nuclear architecture of rod photoreceptor cells adapts to vision in mammalian evolution. *Cell*, **137**, 356–368.

Solovei, I., Thanisch, K. and Feodorova, Y. (2016) How to rule the nucleus: divide et impera. *Curr. Opin. Cell Biol.*, **40**, 47–59.

Sorokin, D.V., Arifulin, E.A., Vassetzky, Y.S. and Sheval, E.V. (2020) Live-Cell Imaging and Analysis of Nuclear Body Mobility. *Methods Mol. Biol.*, **2175**, 1–9.

Sorokin, D.V., Peterlik, I., Tektonidis, M., Rohr, K. and Matula, P. (2018) Non-Rigid Contour-Based Registration of Cell Nuclei in 2-D Live Cell Microscopy Images Using a Dynamic Elasticity Model. *IEEE Trans. Med. Imaging*, **37**, 173–184.

Sparvoli, E., Gay, H. and Kaufmann, B.P. (1965) Number and patterns of association of chromonemata in the chromosomes of *Tradescantia*. *Chromosoma*, **16**, 415–435.

Steensel, B. van and Belmont, A.S. (2017) Lamina-associated domains: Links with chromosome architecture, heterochromatin, and gene repression. *Cell*, **169**, 780–791.

Strukov, Y.G., Wang, Y. and Belmont, A.S. (2003) Engineered chromosome regions with altered sequence composition demonstrate hierarchical large-scale folding within metaphase chromosomes. *J. Cell Biol.*, **162**, 23–35.

Temsch, E.M., Greilhuber, J., Hammett, K.R.W. and Murray, B.G. (2008) Genome size in Dahlia Cav. (Asteraceae–Coreopsideae). *Plant Syst. Evol.*, **276**, 157–166.

Thoma, F., Koller, T. and Klug, A. (1979) Involvement of histone H1 in the organization of the nucleosome and of the salt-dependent superstructures of chromatin. *J. Cell Biol.*, **83**, 403–427.

Van de Peer, Y., Mizrachi, E. and Marchal, K. (2017) The evolutionary significance of polyploidy. *Nat. Rev. Genet.*, **18**, 411–424.

Vejdovsky, F. (1912) Zum Problem der Vererbungsträger. Verlag der Königlich Böhmischen Gesellschaft der Wissenschaften, Prag, 184 pp.

Weisshart, K., Fuchs, J. and Schubert, V. (2016) Structured illumination microscopy (SIM) and photoactivated localization microscopy (PALM) to analyze the abundance and distribution of RNA polymerase II molecules on flow-sorted Arabidopsis nuclei. *Bio-protocol*, **6**, e1725–e1725.

Zatsepina, O.V., Polyakov, V.Y. and Chentsov, Y.S. (1983) Chromonema and chromomere. *Chromosoma*, **88**, 91–97.

Zonneveld, B.J.M., Leitch, I.J. and Bennett, M.D. (2005) First nuclear DNA amounts in more than 300 angiosperms. *Ann. Bot.*, **96**, 229–244.